frontiers in Materials

TYPE Original Research
PUBLISHED 14 September 2026
DOI 10.3389/fmats.2026.1924267

OPEN ACCESS

EDITED BY
Jagpreet Singh,
Rayat Bahra University, India

REVIEWED BY
Diego Carlos Bouttier-Figueroa,
University of Sonora, Mexico
Erdal Ertaş,
Batman University, Türkiye

*CORRESPONDENCE
Yogita Abhale,
mahayogi.85@gmail.com
Suresh Ghotekar,
ghotekarsuresh7@gmail.com

RECEIVED 30 June 2026
REVISED 29 July 2026
ACCEPTED 30 July 2026
PUBLISHED 14 September 2026

CITATION
Thakur A, Patel K, Patil M, Abhale Y, Chavda V, Ravikumar CR and Ghotekar S (2026) Bio-inspired synthesis of $ZnCr_2O_4$ nanoparticles using *Crateva religiosa* leaf extract and their insights into antituberculosis, anticancer and metal sensing properties.
Front. Mater. 13:1924267.
doi: 10.3389/fmats.2026.1924267

Bio-inspired synthesis of $ZnCr_2O_4$ nanoparticles using *Crateva religiosa* leaf extract and their insights into antituberculosis, anticancer and metal sensing properties

Aanshi Thakur[1], Kajalben Patel[1], Mamta Patil[1], Yogita Abhale[1]*, Vishwajit Chavda[2], C. R. Ravikumar[3] and Suresh Ghotekar[4]*

[1]Department of Chemistry, Government College Daman, Daman, India, [2]Department of Environmental Engineering, Kyungpook National University, Daegu, Republic of Korea, [3]Research Centre, Department of Chemistry, East West Institute of Technology, Bangalore, Karnataka, India, [4]Centre for Herbal Pharmacology and Environmental Sustainability, Chettinad Hospital and Research Institute, Chettinad Academy of Research and Education, Chennai, Tamil Nadu, India

The development of eco-friendly nanomaterials has become a major focus in modern nanotechnology due to their wide-ranging applications in biomedical and environmental fields. In the present investigation, zinc chromite nanoparticles ($ZnCr_2O_4$ NPs) were successfully fabricated via a biogenic, sustainable protocol employing *Crateva religiosa* leaf extract as a natural bio-reductant and bio-stabilizer. A variety of analytical methods were used to assess the structural, optical, and functional characteristics of the biosynthesized NPs. A well-defined cubic spinel $ZnCr_2O_4$ phase was confirmed by XRD investigation, and the mean crystallite diameter determined by Scherrer's equation was 15.33 nm. Fourier-transform infrared studies disclosed the typical Zn–O and Cr–O vibrational bands, affirming the successful production of the spinel framework. UV–Visible diffuse reflectance spectroscopy showed a prominent absorption peak around 288 nm, and the optical band gap was estimated to be 1.27 eV. Morphological analysis indicated the formation of flake-like NPs with good surface features. The synthesized $ZnCr_2O_4$ NPs further exhibited moderate anticancer activity, appreciable antitubercular activity, and promising metal-sensing capability toward Cu^{2+} ions. The results of this study demonstrate that the green synthesis method using *Crateva religiosa* extract offers a practical, affordable, and environmentally safe way to produce multifunctional $ZnCr_2O_4$ NPs suitable for biomedical and sensing applications.

KEYWORDS
anticancer, anti-tubercular, *Crateva religiosa*, green synthesis, metal sensor, $ZnCr_2O_4$ NPs

1 Introduction

The rapid advancement of nanotechnology has opened new avenues for scientific innovation and technological development across multiple disciplines (Pushparaj et al., 2022;

GRAPHICAL ABSTRACT

Lu et al., 2016; Lowry et al., 2019; Ghotekar et al., 2024a). Due to their distinctive structural, optical, electrical, and surface-related characteristics that set them apart from their bulk counterparts, nanomaterials (NMs) have garnered significant attention in recent years (Barhoum et al., 2022; Lim et al., 2015; Soni et al., 2025; Chaudhary et al., 2025). These exceptional characteristics have made NMs one of the most dynamic and widely explored areas in modern interdisciplinary research (Qiu et al., 2025; Wang et al., 2024). Owing to their remarkable physicochemical properties, NMs are now widely used in diverse disciplines such as electronics, medicine, cosmetics, catalysis, textiles, optoelectronics, energy storage, environmental remediation, military technologies and sensor development (Yu et al., 2016; El Shafey, 2020; Chavali and Nikolova, 2019; Tural et al., 2026). Their capacity to improve performance, efficiency and sensitivity across a variety of applications has accelerated the global expansion of nanotechnology-based research, making it a major engine of cutting-edge scientific and industrial advancement (Cuong et al., 2022; Ndaba et al., 2022; Demir Becerekli and Akbaş, 2026).

Transition-metal spinel oxides have emerged as an important class of materials in the rapidly developing field of nanoscience and nanotechnology due to their fascinating structural and magnetic properties (Patel et al., 2025a; Patel et al., 2025b; Patil et al., 2025; Ali et al., 2024). These compounds generally possess the chemical formula AB_2X_4, where A and B represent divalent and trivalent metal cations, respectively. These cations exhibit a variety of physical and chemical behaviors due to complicated charge, orbital, and spin interactions caused by their special arrangement inside the spinel lattice. Among chromium-based spinel oxides, $ZnCr_2O_4$ has emerged as a highly promising material owing to its favorable combination of structural robustness, chemical inertness, and versatile functional characteristics. Although $CoCr_2O_4$ has attracted considerable interest because of its ferrimagnetic behavior, its magnetic nature is not essential for many photocatalytic and biomedical applications and may even complicate certain optoelectronic processes. $NiCr_2O_4$ has been extensively investigated for its favorable electronic transport properties and sensing performance; however, precise control over its particle architecture and phase purity remains challenging under many synthesis conditions. Similarly, $CuCr_2O_4$ frequently undergoes lattice distortion arising from the Jahn-Teller effect associated with Cu^{2+} ions, which can influence its crystallographic stability and functional performance. In contrast, $ZnCr_2O_4$ crystallizes in a stable cubic spinel framework that exhibits excellent resistance to thermal and chemical degradation while offering physicochemical properties that can be effectively tailored through controlled synthesis strategies. Moreover, its compatibility with environmentally benign synthetic approaches, together with its demonstrated potential in photocatalysis, chemical sensing, antimicrobial research and cancer therapeutics, makes $ZnCr_2O_4$ an attractive platform for the development of multifunctional NMs. These attributes collectively distinguish $ZnCr_2O_4$ from other chromite spinels and provide a strong rationale for its selection in the present investigation (Patel et al., 2025a; Patel et al., 2025b; Patel et al., 2026).

$ZnCr_2O_4$ exhibits a normal spinel structure in which Zn^{2+} ions occupy tetrahedral (Td) sites and Cr^{3+} ions occupy octahedral (Oh)

TABLE 1 Comparative overview of the synthesis strategies employed for $ZnCr_2O_4$ NMs.

Method	Advantages	Limitations	Ref.
Sol-gel	High purity, homogeneous composition, and controlled particle size	Costly precursors, lengthy process, and calcination required	(Yazdanbakhsh et al., 2010)
Hydrothermal	High crystallinity and morphology control	High-pressure equipment, and long reaction time	(Fu et al., 2023)
Combustion	Rapid, simple, and scalable	Agglomeration and limited morphology control	(Thennarasu and Sivasamy, 2015)
Coprecipitation	Economical, simple, and scalable	Poor crystallinity and broad particle-size distribution	(Fu et al., 2023)
Green synthesis	Eco-friendly, biocompatible, sustainable, and low toxicity	Variation in plant extract composition and reproducibility issues	(Ghotekar et al., 2024b)

sites. The octahedral crystal field around Cr^{3+} splits the 3d orbitals into t_{2g} and, e_g levels, while Zn–O and Cr–O interactions influence the electronic band structure. This specific cation distribution strongly influences the magnetic characteristics of the material, resulting in distinctive magnetic behavior and making $ZnCr_2O_4$ a highly promising material for various technological and biomedical applications (Patel et al., 2026; Choudhary et al., 2017).

Generally, $ZnCr_2O_4$ NPs have been created using both chemical and physical methods as reported in the literature (Patel et al., 2026). The selection of the preparation method plays a pivotal role in governing the phase purity, crystallographic features, microstructure, and physicochemical behavior of the resulting material. As a result, ongoing attempts have been made to create synthetic techniques that offer exact control over these attributes while also enhancing process sustainability and economic viability. Plant-mediated synthesis has drawn more interest recently as an eco-friendly substitute for traditional chemical processes. By employing naturally occurring phytochemicals as reducing and stabilizing agents, this approach minimizes the dependence on hazardous reagents and aligns with the principles of green chemistry. These advantages have stimulated growing interest in the development of eco-friendly $ZnCr_2O_4$ NMs for diverse technological, environmental, and biomedical applications. A comparative summary of the synthesis methods reported for $ZnCr_2O_4$ NPs, together with their major advantages and limitations, is presented in Table 1.

Intriguingly, the synthesis technique significantly influences the physical and chemical properties of the NPs. Modifications in synthesis parameters result in substantial variations in particle size, morphology, crystal structure, and optical properties. Additionally, factors such as calcination temperature, fuel type, reducing agent, and coating material strongly influence nucleation and growth processes. These parameters ultimately determine the final morphology, crystallite size, and electronic characteristics of $ZnCr_2O_4$ NPs as shown in Table 2. Therefore, careful selection and optimization of the synthesis process are essential for tailoring $ZnCr_2O_4$ NPs for specific applications.

Chemical techniques require expensive equipment, specialized personnel to operate the instruments, and potentially dangerous substances that could harm the environment and human health. On the other hand, the green approach addresses environmental issues associated with conventional synthesis processes while offering a sustainable and economical solution by replacing potentially hazardous substances with environmentally favorable alternatives. One-pot synthesis of nature-inspired NPs offers the advantages of low energy consumption, affordability, and integration of environmental, economic, and social considerations (Patel et al., 2023; Rana et al., 2020; Kimta et al., 2025). Green sources play an important role in the synthesis of NPs, as capping and bio-reducing agents confer superior stability on nanoparticles, and nanoparticles synthesized in a green way exhibit variable sizes and morphologies (Jadoun et al., 2021; Shreyash et al., 2021; Ditlopo et al., 2022; Rana et al., 2025; Chauhan et al., 2025). Furthermore, *Crateva religiosa* exhibits substantial pharmacological and nutritional properties owing to the presence of numerous bioactive compounds (flavonoids, phenols, tannins, saponins and terpenoids), which contribute to its potential as a source for developing antimycobacterial and chemotherapeutic agents (Wagay et al., 2017; Ali et al., 2025).

Because of their significant biological activity, $ZnCr_2O_4$ NPs have attracted considerable attention within the biomedical industry. Prior studies have demonstrated the biological applications of $ZnCr_2O_4$ NPs and their composites. These materials have exhibited notable antibacterial and antifungal activities against a wide spectrum of pathogenic microorganisms. Additionally, $ZnCr_2O_4$-based NMs have shown antimalarial activity and significant anticancer effects against various cancer cell lines, including HeLa, MCF-7, and MDA-MB-231. Moreover, $ZnCr_2O_4$-containing composite scaffolds have demonstrated superior wound-healing, antibiofilm, and biocompatibility properties, underscoring their suitability for tissue engineering and wound dressing applications. Overall, these findings suggest that $ZnCr_2O_4$-based NMs possess extensive biomedical potential and merit further investigation for therapeutic use (Patel et al., 2026; Ghotekar et al., 2023; Salehi et al., 2019; Kumari et al., 2022; Peng et al., 2024; Priyanka et al., 2024).

In particular, their anticancer potential has been widely explored due to their potential to produce reactive oxygen species, induce oxidative stress, and trigger apoptosis in cancer cells. Such mechanisms make metal oxide NPs promising candidates

10.3389/fmats.2026.1924267

TABLE 2 $ZnCr_2O_4$ NPs synthesis using various techniques.

Synthesis	Fuels/Reducing agent	Calcination temperature	Characterization techniques	Band gap (eV)	Size (nm)	Morphology	Applications	Ref.
Thermal treatment	1,2-ethanediol	450 ℃–800 ℃	XRD, FE-SEM, HRTEM, and SAED	2.45–2.9	10–30	Round	Photocatalytic activity	(Dumitru et al., 2018)
Sol-gel auto combustion	Urea	500 ℃	UVDRS, XRD, FTIR, HRTEM, EDX, and VSM	3.45	45–80	Hexagonal	Antibacterial, antifungal, and antimalarial activities	(Ghotekar et al., 2023)
Microwave combustion	Citric acid, succinic acid, maleic acid, glycine, and urea	-	UV-vis, XRD, SEM, and HRTEM	1.46–2.22	18.6–13.9	Uneven polyhedron	-	(Sankudevan et al., 2023)
Solvothermal	Yolk-shell	450 ℃	XRD, FESEM, HRTEM, EDS, XPS, and BET	-	2.5 and 1.25 mm	Microsphere	Gas sensor	(Zhao et al., 2023)
Green synthesis	*Hibiscus Rosa Sinensis*	RT, 200, 500 ℃ and 700 ℃	UV-vis-DRS, XRD, FTIR, HRTEM, and SEM	2.47, 2.40, 3.19 and 3.09	~4.52	Cubic	-	(Mayedwa et al., 2021)
	Cow urine	600 ℃	UV-DRS, XRD, IR, XPS, FESEM EDX, and HRTEM	1.8	18.13 (XRD)	Polyhedral	Heterogeneous nanocatalyst	(Ghotekar et al., 2024b)
	Aloe vera	200, 500 ℃ and 700 ℃	PXRD, UV-vis FTIR, SEM, XPS, and TEM	3–2.8	26–32	Hexagonal	Supercapacitors	(Priyanka et al., 2024)
	Crateva religiosa	**600 ℃**	XRD, UV-Vis-DRS, FTIR, SEM-EDS, and TEM-SAED	**1.27**	**15.71**	Uneven-flake	Antituberculosis, anticancer, and metal sensing	Present work

for targeted cancer therapy and drug delivery applications (Patel et al., 2026; Choudhary et al., 2017). $ZnCr_2O_4$ NPs exhibit promising antitubercular activity in addition to anticancer activity. There is a pressing demand for new antimicrobial materials with increased therapeutic efficacy due to the rise of multidrug-resistant strains of *Mycobacterium tuberculosis*. NPs with high surface area and enhanced cellular interaction can effectively inhibit microbial growth, making them attractive materials for antitubercular research (Heidary et al., 2019; Akinnawo and Dube, 2025; Behzad et al., 2022; Simões et al., 2020). Apart from biomedical applications, $ZnCr_2O_4$ NPs also exhibit excellent optical and electronic properties that are highly beneficial for sensing. Spinel zinc chromite materials have shown strong sensitivity to various metal ions due to their efficient charge-transfer capability and surface adsorption behavior. $ZnCr_2O_4$ NPs are good options for sensitive and selective metal ion detection, which is crucial for environmental monitoring and public health protection (Mousavi et al., 2016).

Considering these advantages, the present study focuses on the phytosynthesis of $ZnCr_2O_4$ NPs employing *Crateva religiosa* leaf extract and the evaluation of their structural, optical, anticancer, antitubercular, and metal-sensing properties. The adopted green synthesis strategy offers an environmentally benign and sustainable pathway for the development of multifunctional NMs with potential uses in environmental and biomedical sectors.

2 Experimental

2.1 Materials

AR-grade zinc nitrate hexahydrate ($Zn(NO_3)_2.6H_2O$) and chromium nitrate nonahydrate ($Cr(NO_3)_3.9H_2O$) were utilized as precursor materials for bio-fabrication of $ZnCr_2O_4$ NPs. Fresh leaves of *Crateva religiosa* were collected from a village near Navsari and used to prepare the plant extract, which served as a natural bio-reductant and bio-stabilizer agent in the green synthesis process. Deionized water (dH_2O) was employed as the solvent throughout the experiment. All chemicals employed in this work were of analytical purity and utilized without any additional purification.

2.2 Plant extract preparation

Fresh and healthy *Crateva religiosa* leaves were selected, and 5 g of them were weighed and carefully washed 3–4 times with dH_2O. The cleansed leaves were cut into small pieces and placed in a clean beaker comprising 100 mL of dH_2O. The mixture was heated at 60 °C for 25 min, then allowed to cool to RT. The resulting aqueous extract was filtered through Whatman filter paper (pale yellow). The resulting extract was collected, and the filtrate was utilized for $ZnCr_2O_4$ NP synthesis. Finally, it was stored at 4 °C in a refrigerator for further work. Table 3 shows that the phytochemical analysis identified the presence of terpenoids, flavonoids, tannins, phenolic compounds, carbohydrates, and saponins.

2.3 Synthesis of $ZnCr_2O_4$ NPs

For the biogenic fabrication of $ZnCr_2O_4$ NPs, chromium nitrate nonahydrate and zinc nitrate hexahydrate were dissolved in 30 mL of dH_2O in a 1:2 stoichiometric ratio under continuous magnetic stirring. Following that, 5 mL of aqueous extract of *Crateva religiosa* leaves was mixed dropwise into the mixture, and the mixture was swirled continuously for 30 min. The resulting homogeneous solution was then dried in a hot-air oven to yield a blackish-green dry gel. Finally, the resulting material was calcined in a furnace at 600 °C (2 h). After cooling to room temperature, the calcined product was pulverized with a mortar and pestle to produce fine blackish-colored $ZnCr_2O_4$ NPs. This temperature was chosen based on literature reports and optimization studies because it provides adequate energy for organic residue removal, spinel phase development, and crystallization while reducing particle aggregation. Figure 1 shows the natural extract-assisted eco-friendly synthesis of $ZnCr_2O_4$ NPs.

2.4 Characterization techniques

We used optical, structural, and morphological characterization approaches to study the bio-inspired production of $ZnCr_2O_4$ NPs. The crystallinity and phase formation of $ZnCr_2O_4$ NPs were investigated by X-ray diffraction (XRD; Rigaku). The Fourier-transform infrared (FTIR) spectrum of the $ZnCr_2O_4$ NPs was recorded using a JASCO FTIR-4600 Type A spectrometer employing the KBr pellet method. The FTIR spectrum of the *Crateva religiosa* leaf extract was recorded using a Bruker FTIR spectrometer with a CaF_2 window/sample holder. The optical absorption spectra of produced $ZnCr_2O_4$ NPs were examined using a UV-visible spectrophotometer (Shimadzu DRS-2600). The surface topology and elemental composition were scrutinized employing field-emission scanning electron microscopy (FESEM; Carl Zeiss Model supra55) and energy-dispersive X-ray analysis (EDAX; Quantax 200). The particle size and surface topography were further analyzed employing high-resolution transmission electron microscopy (HRTEM; Talos F200x).

2.5 Anticancer activity

The anticancer activity of synthesized $ZnCr_2O_4$ NPs was evaluated against the human breast cancer cell line MDA-MB-231 using the MTT assay (Hatt et al., 2022). To facilitate cell adhesion, cells were seeded in a 96-well plate at a density of 1×10^2 cells per well and incubated (37 °C) with 5% CO_2 overnight. Following treatment, the cells were cultured for 48 h at varying sample doses (100–3.12 μg/mL). After treatment, the wells were washed with PBS, and 20 μL of MTT solution (5 mg/mL) was poured. Formazan crystal formation was permitted by incubating the plate for 4 hours. 100 μL of DMSO was used to dissolve these crystals, and a microplate reader was employed to quantify absorbance at 570 nm. Cell viability (Equation 1) was computed relative to untreated control cells, and the IC_{50} value was ascertained as the concentration required to reduce cell viability by 50%.

$$\%\text{Viability} = \frac{\text{OD of treated sample}}{\text{OD of control}} \times 100 \quad (1)$$

2.6 Antitubercular activity

The antitubercular activity of $ZnCr_2O_4$ NPs was tested against *Mycobacterium tuberculosis* H37Rv using the Microplate

TABLE 3 Phytochemicals present in the aqueous extract of the *Crateva religiosa* leaf.

Test	Phytochemical	Role in $ZnCr_2O_4$ synthesis
Foam froth test	Saponin	Surface stabilization and particle dispersion
Ninhydrin test	Amino acid	Coordination and precursor stabilization
Lead acetate test	Phenol	Chelation of Zn^{2+}/Cr^{3+}, stabilization
Alkaline reagent test	Flavonoids	Metal complexation and nucleation control
Gelatin Test	Tannins	Strong capping agent, inhibits agglomeration
Salkowski test	Terpenoids	Weak reducing and stabilizing agent

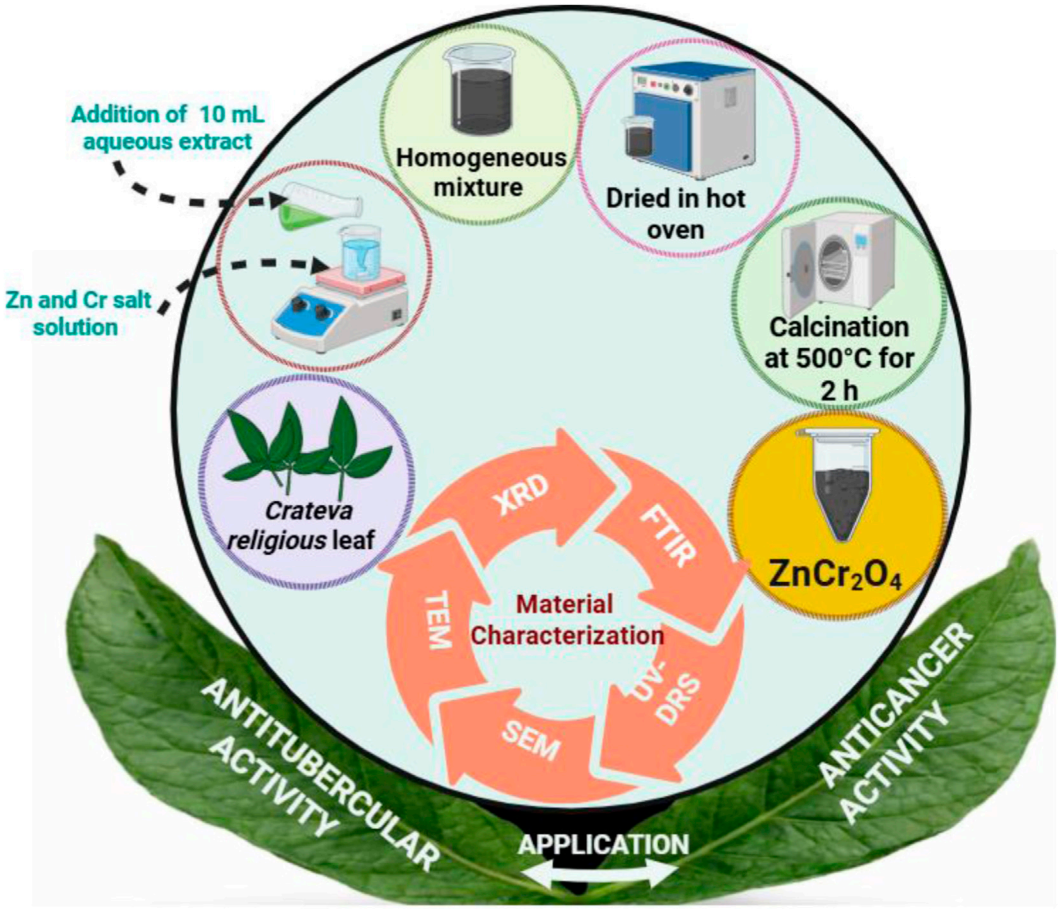

FIGURE 1
Graphical representation of the phytosynthesis of $ZnCr_2O_4$ employing *Crateva religiosa* extracts (www.biorender.com).

Alamar Blue Assay (MABA) (Lourenco et al., 2007). To prevent evaporation, sterile water was poured into the outer wells of a 96-well plate containing bacterial cultures in Middlebrook 7H9 broth. After adding serial dilutions of the samples (100–0.2 μg/mL), the plates were incubated for 5 days (37 °C). After incubation, a mixture of Alamar Blue reagent and 10% Tween-80 was poured, and the plate was incubated for a further 24 h. A pink hue indicated bacterial growth, while a blue hue indicated inhibition. The lowest concentration that stopped the color shift was noted as the minimum inhibitory concentration (MIC).

3 Results and discussion

3.1 XRD study

XRD was used to analyze the phase formation, purity, and crystallinity of the *Crateva religiosa*-assisted $ZnCr_2O_4$ NPs. The XRD pattern is illustrated in Figure 2. The diffraction peaks corresponded to the cubic spinel structure of $ZnCr_2O_4$ with the space group Fd-3 m (227), as per ICDD card no. 22–1,107 (Mousavi et al., 2016). The diffraction peaks align with the (111) (220) (311) (222) (400) (422) (511) (440) (531) (620), and (533) crystallographic planes,

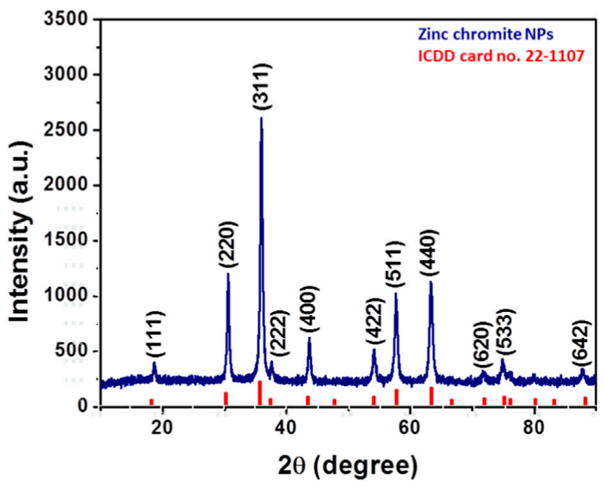

FIGURE 2
XRD profile of *Crateva religiosa* leaf extract-mediated $ZnCr_2O_4$ NPs.

with 2θ values ranging from 18.64° to 87.58°. Among all the diffraction peaks, the intense peak corresponding to the (311) plane indicates the preferential orientation and high crystallinity of the synthesized NPs. The presence of sharp, distinct diffraction peaks suggests that the synthesized material is highly crystalline. At the same time, the slight broadening of the peaks indicates the formation of particles in the nm range. No additional diffraction peaks attributable to impurities or secondary phases were observed, confirming the purity of the as-produced $ZnCr_2O_4$ NPs. The results clearly suggest that the biomolecules present in the *Crateva religiosa* extract effectively assisted in reducing and stabilizing the NPs during the biogenic synthesis. The average crystallite size of $ZnCr_2O_4$ NPs was determined using Scherrer's equation, yielding 15.33 nm (Ghotekar et al., 2024b). The mean crystallite size was calculated using Scherrer's equation (Equation 2). Here, D is the average crystallite size, K is the shape factor (typically 0.9), λ is the X-ray wavelength (1.5406 Å for Cu Kα), β is the full width at half maximum (FWHM) of the diffraction peak in radians after correcting for instrumental broadening, and θ is the Bragg diffraction angle (Holzwarth and Gibson, 2011).

$$D_{hkl} = \frac{K\lambda}{\beta \cos \theta} \tag{2}$$

3.2 UV-DRS

The optical nature of the green-synthesized $ZnCr_2O_4$ NPs was examined by utilizing UV–Vis diffuse reflectance spectroscopy (DRS). The spectrum displayed a distinct absorption peak near 288 nm (Figure 3a), confirming the successful formation of $ZnCr_2O_4$ NPs. This absorption behavior can be attributed to electronic interactions between the band electrons and the d-orbitals of Cr^{3+} and Zn^{2+} ions. Such sp–d exchange interactions are known to influence the electronic structure of the material by causing slight shifts in both the valence and conduction bands, thereby affecting the optical response of the NPs. Direct transitions occur between band extrema at the same crystal momentum and involve only a photon. This gives a strong, sharp absorption edge. Indirect transitions involve a change in crystal momentum and require a phonon. This results in a weaker, more gradual edge (Sankudevan et al., 2023). To further evaluate the optical characteristics, the band gap energy was estimated from a Tauc plot assuming a direct allowed transition, by plotting $(\alpha h\nu)^2$ versus photon energy $h\nu$ derived from the DRS data and extrapolating the linear region to the energy axis. The calculated band gap of the $ZnCr_2O_4$ NPs was found to be approximately 1.27 eV (Figure 3b), which is lower than previously reported values by Sankudeven et al. (1.46–2.22 eV) (Sankudevan et al., 2023), Ghotekar et al. (1.80 eV and 3.45 eV) (Ghotekar et al., 2024b) (Ghotekar et al., 2023), Priyanka et al. (2.8–3.0 eV) (Priyanka et al., 2024), and Dumitru et al. (2.45–2.90 eV) (Dumitru et al., 2018), as shown in Table 2. These variations are primarily due to differences in synthesis methods, precursor chemistry, reducing or fuel agents, calcination conditions, crystallite size, morphology, crystallinity, and defect concentration, all of which affect the electronic band structure and optical properties of $ZnCr_2O_4$ NPs.

3.3 FTIR

The FTIR spectrum of *Crateva religiosa* leaf extract displays a broad absorption band at 3,693 cm^{-1}, which corresponds to O–H stretching vibrations of hydrogen-bonded hydroxyl groups found in phenols and alcohols. The absorption at 3,048 cm^{-1} is attributed to aromatic = C–H stretching vibrations, indicating the presence of aromatic phytochemicals. A prominent band at 1735 cm^{-1} corresponds to C=O stretching vibrations of carbonyl-containing compounds, including esters, aldehydes, ketones, or carboxylic acids. The band at 1,576 cm^{-1} is associated with aromatic C=C stretching vibrations, confirming the presence of polyphenolic constituents (Vignesh et al., 2025). The absorption band at 1,102 cm^{-1} is assigned to C–O stretching vibrations of alcohols, ethers, or glycosidic linkages, which suggests the presence of carbohydrates and other oxygenated phytochemicals potentially involved in nanoparticle synthesis and stabilization (Figure 4a) (Anjum et al., 2025) (Tural et al., 2026).

The FTIR spectrum of the $ZnCr_2O_4$ NPs reveals the presence of characteristic functional groups and metal–oxygen interactions associated with the formation of the spinel structure. Two strong peaks, corresponding to the stretching vibrations of Cr–O and Zn–O bonds, were seen in the lower wavenumber area at 525 cm^{-1} and 629 cm^{-1}, respectively. The successful development of the $ZnCr_2O_4$ spinel framework is firmly confirmed by the existence of these distinctive peaks (Ghotekar et al., 2023). Furthermore, the bands at 430–495 cm^{-1} represent the stretching vibrations of metal-oxygen bonds (Figure 4b) (Gene et al., 2014).

However, the comparative study of the FTIR spectra of *Crateva religiosa* leaf extract and $ZnCr_2O_4$ NPs is discussed in Table 4.

3.4 SEM and EDAX analysis

The topology and size of $ZnCr_2O_4$ NPs were analyzed employing SEM, as displayed in Figure 5a. The SEM image discloses that the produced NPs have an uneven, flake-like shape and substantial aggregation. The particles appear crowded, resulting in a rough, varied surface texture. Elemental mapping in Figure 5b assesses

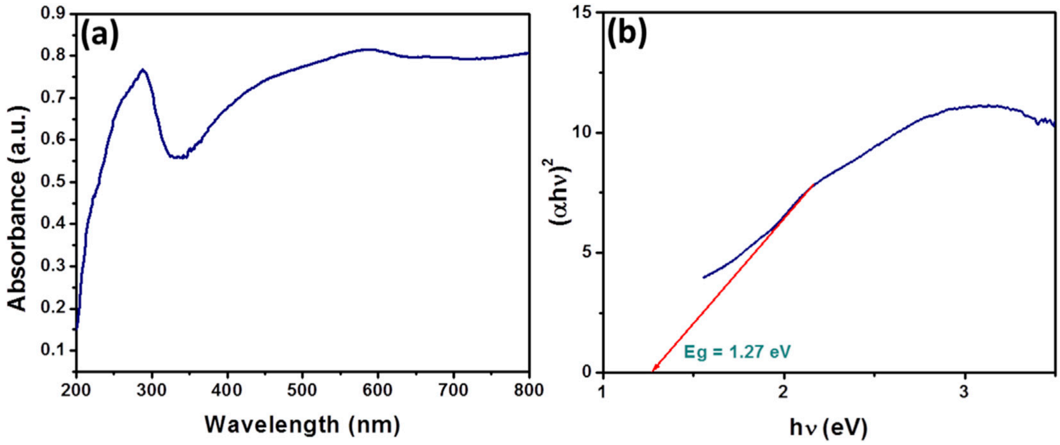

FIGURE 3
(a) UV-vis spectrum of $ZnCr_2O_4$ NPs and **(b)** Band gap of the as-produced $ZnCr_2O_4$ NPs determined employing Tauc's plot.

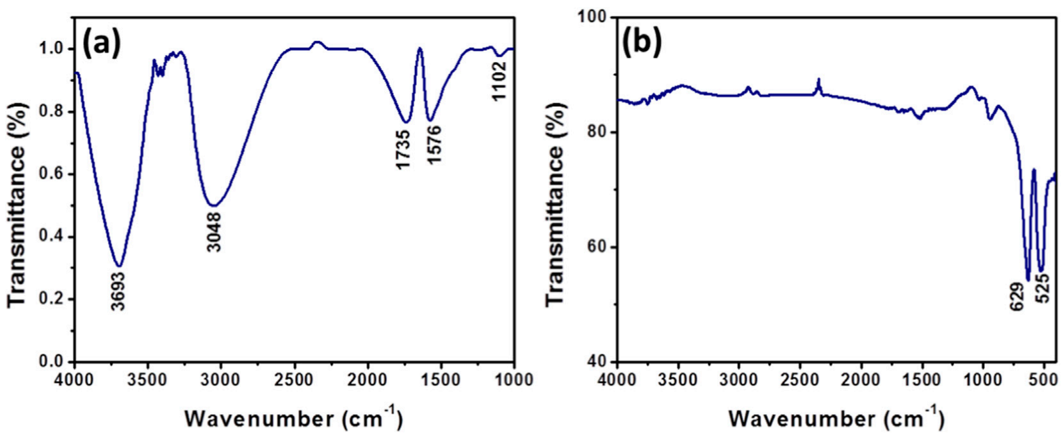

FIGURE 4
(a) FTIR spectra of *C. religiosa* leaf extract and **(b)** *C. religiosa*-mediated $ZnCr_2O_4$ NPs.

the chemical composition and uniform distribution of constituent elements in the produced $ZnCr_2O_4$ NPs. Figure 5c shows the EDAX spectrum of $ZnCr_2O_4$ NPs. Figure 5d shows the homogeneous distribution of Zn, O, and Cr elements. Zn, Cr, and O account for 17.5%, 43.4%, and 39.1% of the weight, respectively. No additional elements were found, indicating that the produced substance was pristine.

3.5 HRTEM analysis

TEM was employed to evaluate the material's nanostructural characteristics and provide extensive insights into its structure and crystallinity. Figure 6a demonstrates that the produced $ZnCr_2O_4$ comprises cuboidal nanoparticles, which are consistent with the SEM images. The NPs had a mean diameter of 15.71 nm, as revealed by the TEM image (Figure 6a) and the particle-size distribution histogram (Figure 6d). The material is crystalline, with well-defined parallel lattice fringes and an estimated interplanar spacing of 0.17 nm between adjacent planes in the HRTEM picture shown in Figure 6b. According to the JCPDS database, this lattice spacing fully matches the (422) crystallographic plane of $ZnCr_2O_4$ NPs. Furthermore, the selected area electron diffraction (SAED) pattern discloses various bright spots forming concentric rings, indicating that the nanocrystals are oriented in multiple orientations (Figure 6c). The SAED pattern shows diffused concentric rings due to electron diffraction, corresponding to the (111) (220) (311) (400) (422) (440), and (620) planes of $ZnCr_2O_4$. These results are consistent with the XRD study (Ghotekar et al., 2024b).

3.6 A possible mechanism for the green production of $ZnCr_2O_4$ NPs

Table 3 outlines the active phytochemicals found in *Crateva religiosa* leaves that help turn zinc and chromium precursor salts into $ZnCr_2O_4$ NPs. The suggested reaction process demonstrates the phytochemicals' reducing, complexing, and stabilizing roles in nanoparticle production. *C. religiosa* leaves contain several bioactive substances, including terpenoids, saponins, flavonoids,

TABLE 4 Compares the FTIR spectra of *C. religiosa* leaf extract and *C. religiosa*-mediated $ZnCr_2O_4$ NPs, with possible band assignments and interpretations.

Crateva religiosa leaf extract (Figure 4a)	*Crateva religiosa*-mediated $ZnCr_2O_4$ NPs (Figure 4b)	Functional group	Interpretation
3,693 cm^{-1}	-	O–H stretching vibrations (Phenols, flavonoids, or absorbed H_2O)	The reduction after synthesis indicates the participation of hydroxyl groups in NPs formation
3,048 cm^{-1}	-	C–H stretching vibrations (organic compounds)	Its disappearance suggests the removal of organic molecules during NPs formation via calcination
1735	-	C=O stretching (aldehydes, ketones, esters, or carboxylic acids)	The disappearance indicates that carbonyl-containing phytochemicals were participated in the reduction/complexation process
1,576	-	C=C aromatic skeletal vibrations	The decrease confirms the interaction of phytochemicals with Zn^{2+} and Cr^{3+} ions
1,102	-	C–O or C–O–C stretching vibrations (alcohols, ethers, or polysaccharides)	Its disappearance indicates that these functional groups were involved in the NPs synthesis
-	525 cm^{-1}	Cr–O bonds	$ZnCr_2O_4$ lattice vibrations confirm successful formation of NPs
-	629 cm^{-1}	Zn–O bonds	

polyphenols, and phenols. Flavonoids and polyphenolic compounds were identified as typical biomolecules to propose a probable reaction mechanism due to their strong metal-chelating and reducing properties (Munir et al., 2021; Roy et al., 2019). Flavonoid aromatic hydroxyl groups bind with Zn^{2+} and Cr^{3+} ions, forming stable metal-flavonoid complexes. During synthesis, these phytochemicals reduce metal ions via electron donation while also adsorbing onto the nanoparticle surface, acting as natural capping and stabilizing agents. This inhibits particle agglomeration and promotes the creation of uniformly dispersed NPs. Calcination causes thermal breakdown of organic compounds, yielding solid $ZnCr_2O_4$ NPs (Figure 7). The aqueous leaf extract of *C. religiosa* contains flavonoids and polyphenolic compounds that serve as reducing and capping agents in the green synthesis of $ZnCr_2O_4$NPs, consistent with previous studies (Vignesh et al., 2025; Rajendaran et al., 2019).

3.7 Anticancer efficacy

The anticancer potential of $ZnCr_2O_4$ NPs was assessed against the MDA-MB-231 (human breast cancer) cell line using the MTT assay, with doxorubicin serving as the reference drug. The results disclosed a clear dose-dependent reduction in cell viability for both treatments. $ZnCr_2O_4$ NPs reduced cell viability to around 36% at the highest tested concentration (100 μg/mL), whereas doxorubicin showed a greater cytotoxic effect, reducing viability to about 17%. As the concentration decreased to 3.125 μg/mL, cell viability gradually increased, reaching nearly 97% for $ZnCr_2O_4$ NPs and approximately 58% for doxorubicin, as shown in Figure 8. Doxorubicin's significant anticancer potency was demonstrated by its computed IC_{50} value of 3.46 μg/mL. $ZnCr_2O_4$ NPs, on the other hand, demonstrated relatively modest cytotoxic activity against MDA-MB-231 cells, as evidenced by an IC_{50} of 72.99 μg/mL (Table 5). Overall, while the NPs displayed measurable anticancer effects, their efficacy remained lower than that of the standard chemotherapeutic agent doxorubicin. $ZnCr_2O_4$ (15.7 nm) is optimally sized for endocytosis, resulting in effective intracellular accumulation. A limitation of this study is that cytotoxicity was assessed only in the MDA-MB-231 breast cancer cell line. Further research using additional cancer and normal cell lines is needed to confirm the NPs broad-spectrum efficacy and selectivity. The nanoscale particle size facilitates cellular uptake via endocytosis, thereby increasing intracellular accumulation and therapeutic efficacy. The narrow bandgap (1.27 eV) enables efficient light-induced separation of electron–hole pairs, thereby increasing the production of reactive oxygen species (ROS) such as hydroxyl and superoxide radicals. These ROS thereby increase mitochondrial dysfunction, DNA damage, and apoptosis in cancer cells. Together, the optimal particle size and narrow bandgap enhance photocatalytic ROS generation and contribute to the promising anticancer activity of $ZnCr_2O_4$ NPs (He et al., 2024; Zeng et al., 2025). Overall, while the $ZnCr_2O_4$ NPs displayed measurable anticancer effects, their efficacy remained lower than that of the standard chemotherapeutic agent doxorubicin.

Although the molecular basis of the observed cytotoxicity was not investigated in the present study, the anticancer activity of $ZnCr_2O_4$ NPs is likely associated with oxidative stress-mediated apoptosis, a mechanism commonly reported for metal oxide

10.3389/fmats.2026.1924267

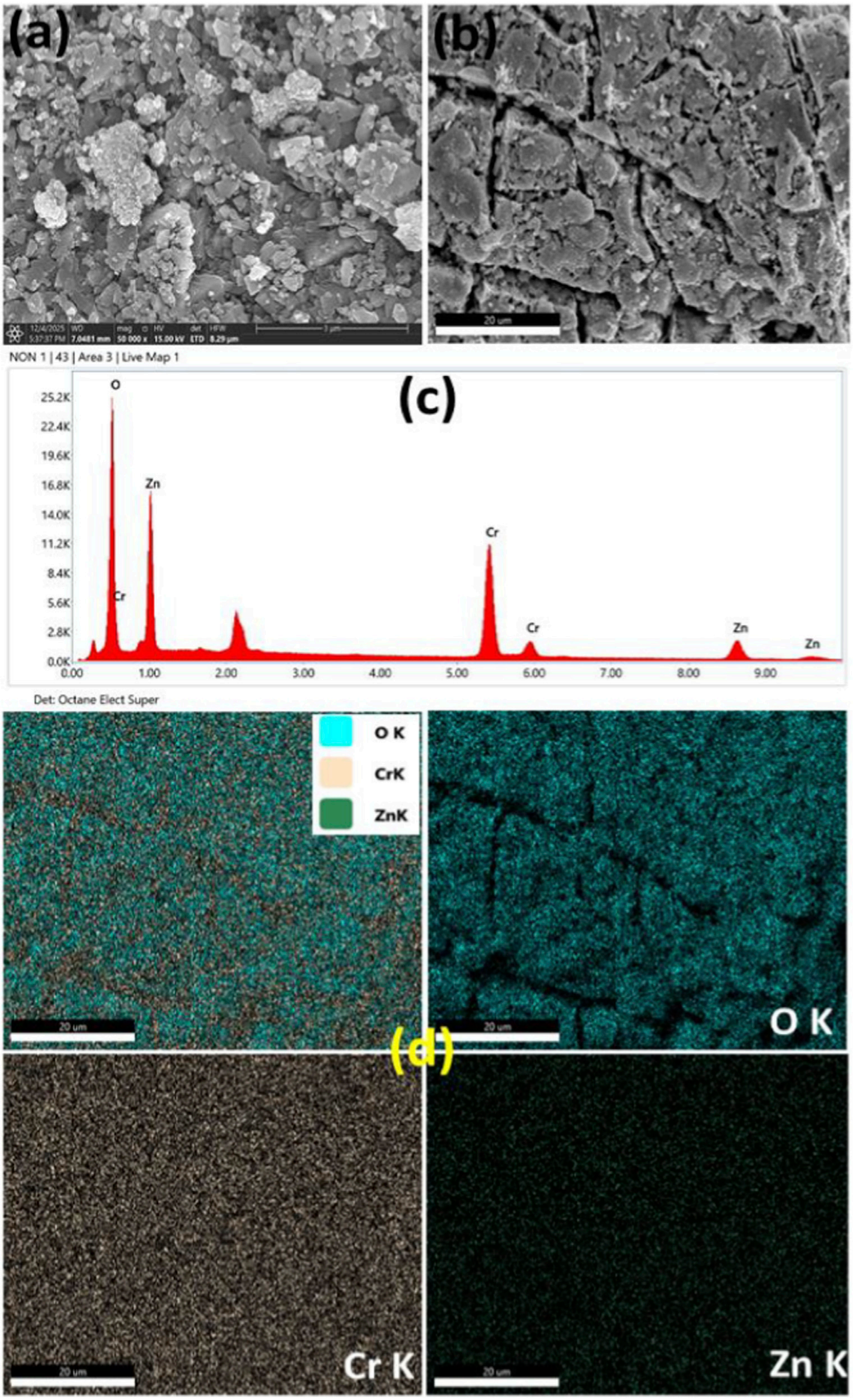

FIGURE 5
(a) SEM images of the as-produced $ZnCr_2O_4$ NPs, **(b)** FESEM image, **(c)** EDAX spectrum, and **(d)** Elemental mapping.

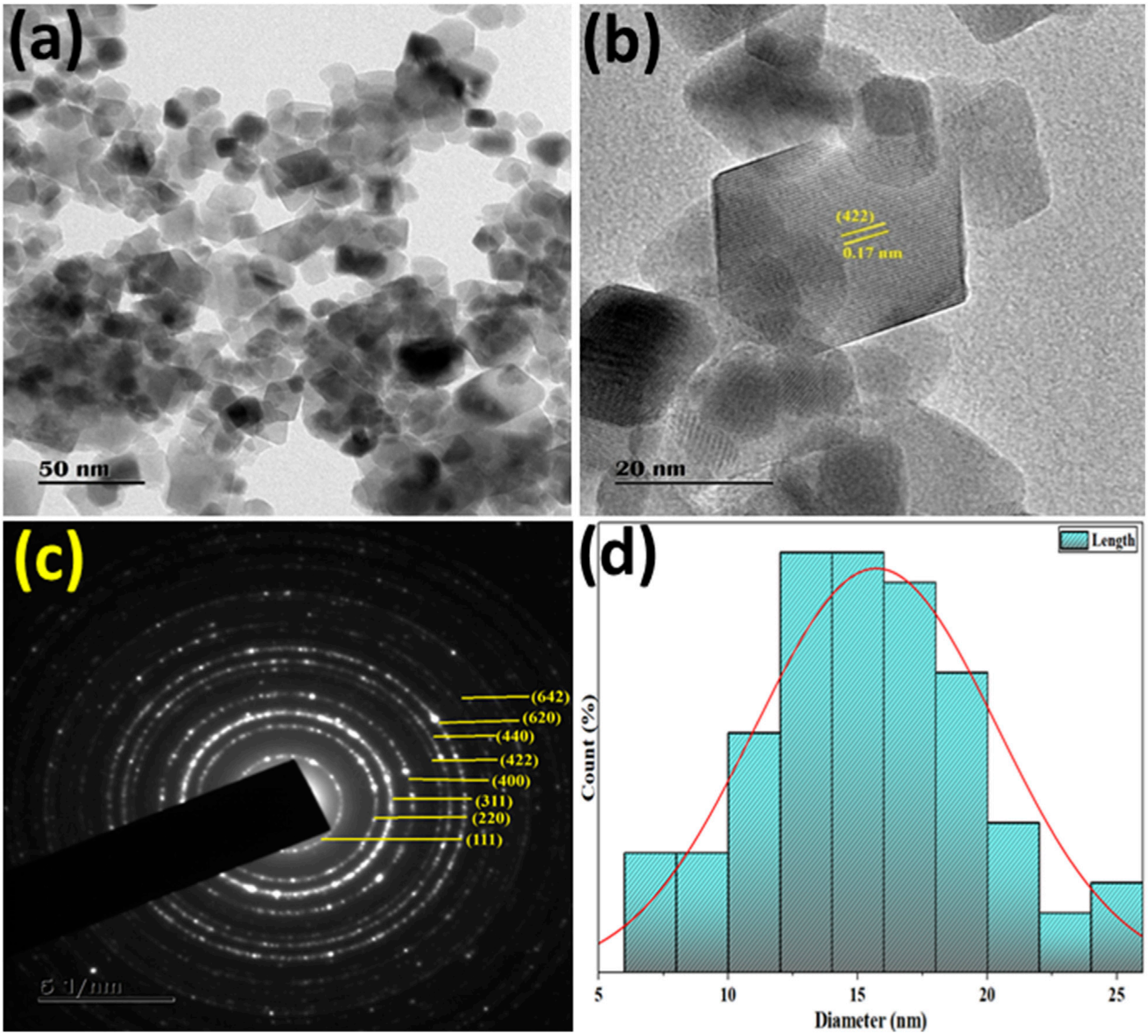

FIGURE 6
TEM images of $ZnCr_2O_4$ at different resolutions of **(a)** 50 nm, **(b)** HRTEM image showing (422) lattice plane with d-spacing 0.17 nm, **(c)** SAED pattern, and **(d)** histogram of particle size distribution.

NMs. The NPs may cause excessive intracellular ROS during cellular internalization, upsetting redox equilibrium and oxidatively damaging vital biomolecules. Through the release of cytochrome c and the subsequent activation of caspase-9 and caspase-3, the ensuing mitochondrial malfunction can initiate the intrinsic apoptotic cascade, which eventually results in programmed cell death. Nevertheless, further investigations involving ROS quantification, mitochondrial membrane potential analysis, and apoptosis assays are required to validate the underlying molecular mechanism (Figure 9) (Priyanka et al., 2024; Anjum et al., 2021; Elmore, 2007).

3.8 Antitubercular activity

The antitubercular potential of the synthesized $ZnCr_2O_4$ NPs was investigated against *Mycobacterium tuberculosis*- H37Rv. The NPs exhibited a notable ability to inhibit bacterial growth, indicating promising antimycobacterial properties. The results are summarized in Table 6. This activity may be linked to the production of reactive oxygen species or the interaction of nanoparticles with the bacterial cell wall, which can impair vital cellular processes and ultimately prevent bacterial viability. For comparison, commonly used first-line antitubercular drugs such as Isoniazid, Ethambutol, Pyrazinamide, Rifampicin, and Streptomycin demonstrated stronger antibacterial performance due to their well-established mechanisms that specifically target vital metabolic pathways of *Mycobacterium tuberculosis*. Figure 10 shows the colorimetric shift from blue to pink in the MABA assay, indicating metabolic activity. Although the activity of $ZnCr_2O_4$ NPs is lower than that of these conventional drugs, the results still highlight their potential as alternative NMs for future antimicrobial research.

FIGURE 7
A potential mechanistic approach for the environmentally benign generation of $ZnCr_2O_4$ NPs.

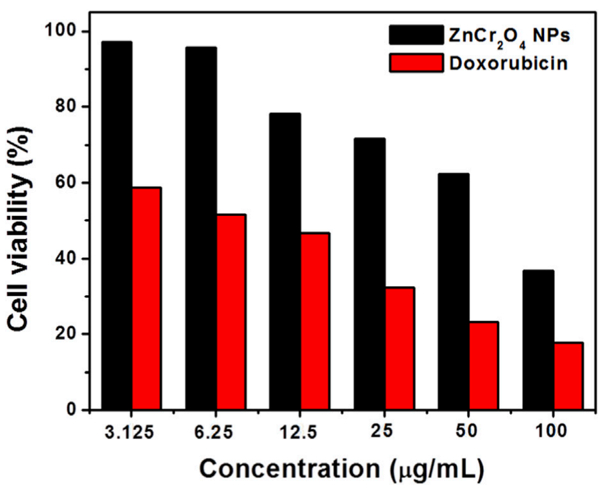

FIGURE 8
Anticancer activity of $ZnCr_2O_4$ NPs against MDA-MB-231 cancer cell line.

To provide a possible explanation for the observed antitubercular activity, a proposed mechanism of action of $ZnCr_2O_4$ NPs against *Mycobacterium tuberculosis* is illustrated in Figure 11. Owing to their high surface area and surface reactivity, $ZnCr_2O_4$ NPs are expected to interact with the mycolic acid-rich bacterial cell envelope, promoting the generation of ROS. The resulting oxidative stress may cause DNA damage, protein oxidation, and lipid peroxidation, which would compromise membrane integrity and increase cellular permeability. Furthermore, $ZnCr_2O_4$ NPs may disrupt vital metabolic processes and limit ATP synthesis by interfering with membrane-associated respiratory enzymes. The combined effects of oxidative stress, membrane damage and metabolic dysfunction are likely to inhibit bacterial growth and ultimately result in cell death (Akinnawo and Dube, 2025; Behzad et al., 2022; Chen et al., 2019). Although these mechanisms were not experimentally investigated in the present study, they are consistent with the reported antimicrobial behavior of metal oxide NPs and provide a plausible explanation for the observed antitubercular activity.

TABLE 5 Anticancer effect of $ZnCr_2O_4$ NPs.

Cell line	Method	Concentration (μg/mL)	Cell viability%	IC_{50} μg/mL	Ref.
MCF-7	MTT assay	1,000	8.77	107	(Wani et al., 2024)
HeLa cells		1,000	6.89	104	
MDA-MB-231		$ZnCr_2O_4$: Ce (9 mol%)	74	-	(Priyanka et al., 2024)
MDA-MB-231		**100**	**36.65**	**72.99**	Present work

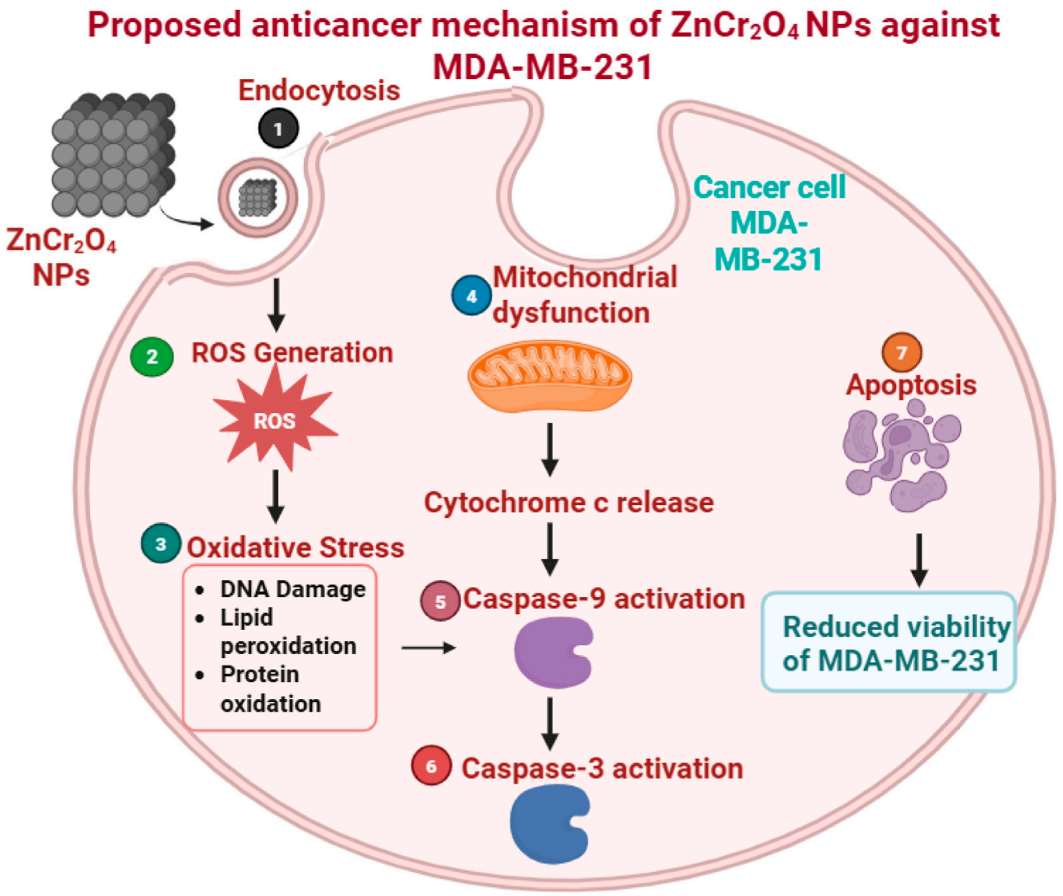

FIGURE 9
Proposed anticancer mechanism of the as-prepared $ZnCr_2O_4$ NPs against MDA-MB-231 cancer cell line (www.biorender.com).

TABLE 6 Antitubercular efficacy of $ZnCr_2O_4$ NPs.

Sample	Concentration (μg/mL)								MIC (μg/mL)
	100	50	25	12.5	6.25	3.2	1.6	0.8	
$ZnCr_2O_4$ NPs	S	S	S	S	S	R	R	R	6.25
Streptomycin	-	-	-	-	-	-	-	-	0.8
Rifampicin	-	-	-	-	-	-	-	-	0.8
Pyrazinamide	-	-	-	-	-	-	-	-	3.125
Ethambutol	-	-	-	-	-	-	-	-	1.6
Isoniazid	-	-	-	-	-	-	-	-	1.6

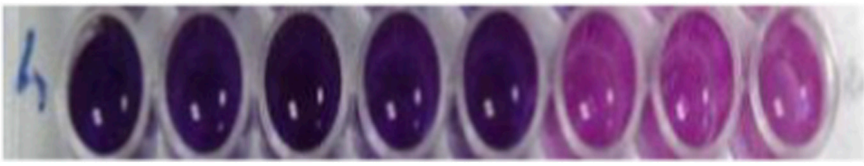

FIGURE 10
Antituberculosis activity of $ZnCr_2O_4$ NPs.

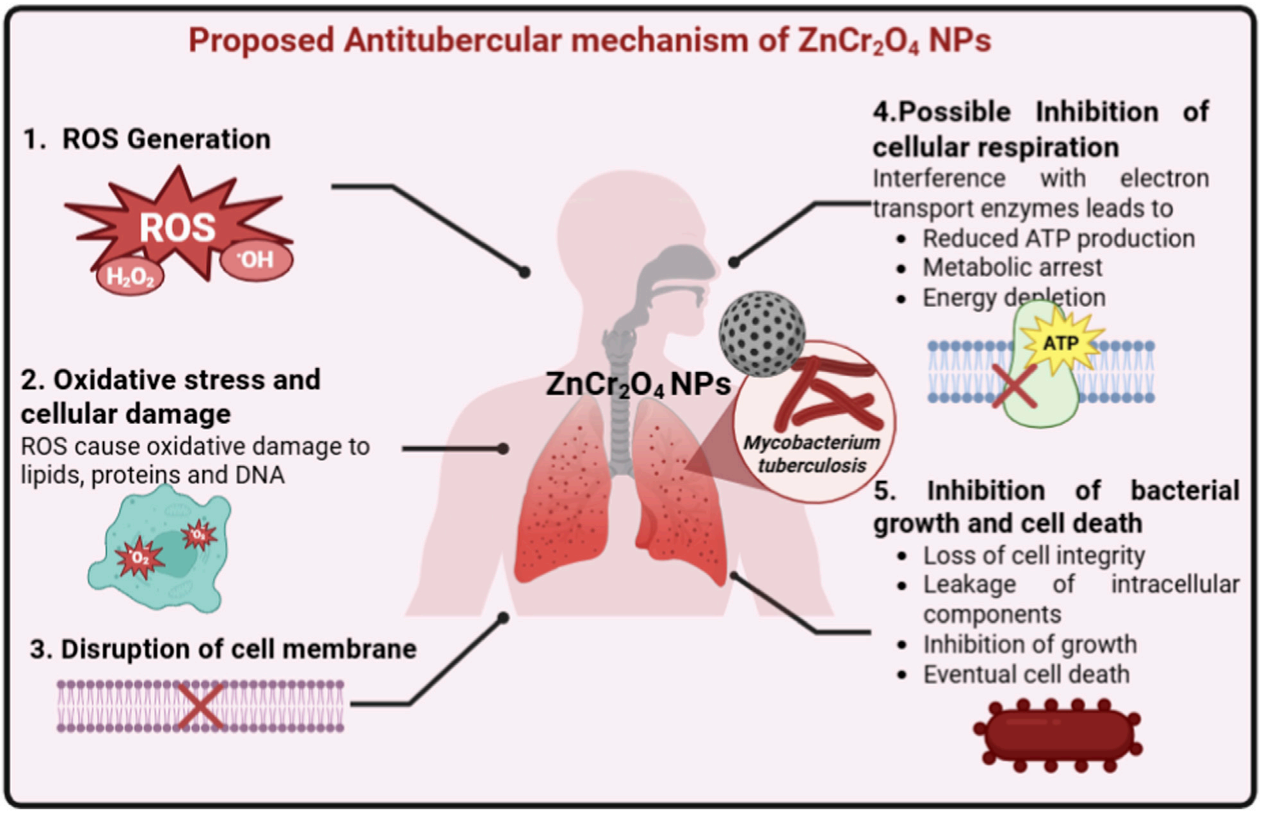

FIGURE 11
Proposed antitubercular mechanism of *C. religiosa*-mediated $ZnCr_2O_4$ NPs (www.biorender.com).

3.9 Metal sensor

The sensor's metal-ion sensing performance was assessed utilizing Perkin-Elmer equipment and bio-inspired *C. religiosa*-mediated $ZnCr_2O_4$ NPs. Metal perchlorate salts were prepared by dissolving metal salts in perchloric acid ($HClO_4$). These solutions were then used in sensing investigations. A 2 mL aliquot of 0.056 mM metal perchlorate solution, including Ba^{2+}, Ca^{2+}, Mg^{2+}, Ni^{2+}, Zn^{2+}, Cu^{2+}, and Cd^{2+} ions, was generated using conductivity-grade water. $ZnCr_2O_4$ NPs were ultrasonically dispersed in conductivity-grade water to create a homogeneous colloidal suspension. The colloidal liquid was filtered via a 0.22 µm syringe filter to remove larger aggregates and achieve uniform nanoparticle dispersion. To study the interaction between metal ions and $ZnCr_2O_4$ NPs, 2 mL of the metal-ion solution was poured with 2 mL of the filtered $ZnCr_2O_4$ nanoparticle suspension. The resulting mixture was evaluated during sensing experiments.

The pristine $ZnCr_2O_4$ NPs show a strong absorption band at about 273 nm and a broad band in the 349–395 nm region, which may be attributed to $O^{2-} \rightarrow Cr^{3+}$ charge-transfer transitions and crystal-field-related electronic transitions within the spinel lattice (Figure 12) (Cherifi et al., 2019). The UV-Vis spectra were used to estimate the optical band gap of $ZnCr_2O_4$, which was found to be 3.55 eV for the direct transition (Choudhary et al., 2017). Treatment with Mg^{2+}, Ca^{2+}, and Ba^{2+} resulted in only minimal modifications, indicating limited interaction with the $ZnCr_2O_4$ framework. The absorption spectra were mildly altered by Ni^{2+}, possibly due to local disruption of the crystal-field environment. This behavior is consistent with studies indicating that Ni-containing oxide systems undergo structural and electronic alterations upon Ni

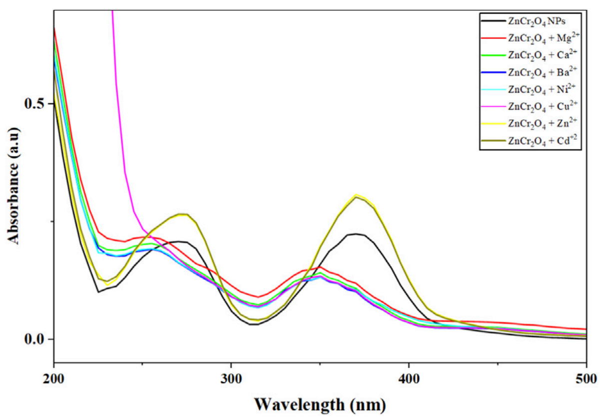

FIGURE 12
Metal ions influence the UV-Vis spectra of $ZnCr_2O_4$ NPs.

incorporation (Kumar et al., 2025). Cu^{2+} exhibits coordination-sensitive optical behavior, resulting in the most significant shift in absorption profile (Qiu et al., 2015). Zn^{2+} and Cd^{2+} exhibited minimal UV-Vis spectrum alterations, indicating poor surface contact and small structural perturbations. Both ions are d^{10} species; therefore, their response is unlikely to involve normal d-d transitions (Tharakeswar et al., 2012). $ZnCr_2O_4$ NPs are a suitable sensing material because they exhibit clear UV-Vis reactions to metal ions, especially Cu^{2+}, but show smaller changes for other ions. Cu^{2+} ions bond to oxygen-containing functional groups on the $ZnCr_2O_4$ nanoparticle surface, inducing electron transfer and a shift in UV-Vis absorbance. Likewise, according to Amigoni-Gerbier et al., cyclam-functionalized nanolatex (NLCyc) binds other metal ions, including Zn^{2+} and Ni^{2+}, while retaining good selectivity for Cu^{2+} (Amigoni-Gerbier et al., 2002). This allows for selective Cu^{2+} detection. Meallet-Renault et al. developed latex nanoparticle-based fluorescent sensors that can detect Cu^{2+} at nanomolar levels. The sensors use a cyclam probe and a Mes-BODIPY fluorophore that are not covalently linked (Meallet-Rena et al., 2006). Their sensing behavior is most likely due to surface contact and coordination-dependent optical modification, making them ideal for optical metal-ion detection.

4 Future prospects

Despite the encouraging findings obtained in the present study, several scientific and technological challenges must be overcome before green-synthesized $ZnCr_2O_4$ NPs can be translated into practical applications. A major priority should be establishing standardized synthesis protocols that ensure consistent phytochemical composition, thereby improving reproducibility and reducing variations associated with plant-derived reducing and capping agents. Moreover, comprehensive optimization of synthesis variables, including precursor stoichiometry, reaction conditions, extract preparation and post-synthesis thermal treatment, is essential for achieving precise control over the structural, morphological and functional characteristics of $ZnCr_2O_4$ NPs while facilitating scalable production.

Further investigations are also warranted to elucidate the molecular mechanisms responsible for the biological activity of $ZnCr_2O_4$ NPs. Specifically, comprehensive omics-based investigations, apoptosis-related signaling networks, intracellular reactive oxygen species production, and mitochondrial malfunction would offer important insights into their anticancer mechanism of action. Systematic *in vivo* assessments of biodistribution, pharmacokinetics, biodegradation, immunological reactions, and long-term biosafety are equally crucial for determining their appropriateness for clinical use. Furthermore, rational surface engineering using biocompatible coatings or disease-specific targeting ligands may increase cellular absorption, reduce negative effects on healthy tissues, and improve therapeutic selectivity.

Beyond the biomedical domain, $ZnCr_2O_4$ NPs possess considerable potential for next-generation technologies owing to their unique physicochemical characteristics. Future efforts should focus on designing hybrid nanostructures, heterojunction systems and defect-engineered architectures to enhance charge-carrier separation, interfacial charge transport and surface reaction kinetics. Such modifications are expected to significantly improve their performance in photocatalysis, environmental remediation, chemical sensing and energy-related devices. Continued progress in these areas will not only expand the application horizon of $ZnCr_2O_4$ NPs but also accelerate their transition from proof-of-concept laboratory studies to sustainable, high-performance technologies with tangible industrial and biomedical relevance.

5 Conclusion

The present study affirms that green synthesis is an effective strategy for producing functional $ZnCr_2O_4$ NPs with enhanced physicochemical and biological properties. The phytochemical constituents of the extract served as natural reducing and stabilizing agents, contributing to the formation of well-crystalline, flake-like NPs with favorable semiconducting properties. The multifunctional performance of the synthesized $ZnCr_2O_4$ NPs was demonstrated through their anti-tubercular, anticancer, and Cu^{2+} sensing capabilities. Among these, the anti-tubercular activity represents the most promising outcome, as evidenced by the low minimum inhibitory concentration against *Mycobacterium tuberculosis*, indicating the potential of these nanoparticles for future anti-TB therapeutic development. Likewise, the selective detection of Cu^{2+} highlights their suitability for environmental monitoring and analytical sensing applications. In contrast, although the NPs exhibited measurable cytotoxicity towards MDA-MB-231 breast cancer cells, their anticancer efficacy remained moderate compared with the reference drug doxorubicin. Consequently, further mechanistic investigations, surface engineering, and comprehensive *in vivo* studies are required before their biomedical potential can be fully established. Collectively, these findings demonstrate that green-synthesized $ZnCr_2O_4$ NPs constitute a promising multifunctional nanomaterial with considerable potential for anti-tubercular and sensing applications. In contrast, their application in cancer therapy warrants further optimization and biological validation.

Data availability statement

The original contributions presented in the study are included in the article/supplementary material, further inquiries can be directed to the corresponding authors.

Ethics statement

Ethical approval was not required for the studies on humans in accordance with the local legislation and institutional requirements because only commercially available established cell lines were used. Ethical approval was not required for the studies on animals in accordance with the local legislation and institutional requirements because only commercially available established cell lines were used.

Author contributions

AT: Conceptualization, Methodology, Writing – original draft. KP: Conceptualization, Data curation, Formal Analysis, Writing – original draft. MP: Conceptualization, Data curation, Formal Analysis, Writing – original draft. YA: Methodology, Project administration, Supervision, Writing – review and editing. VC: Formal Analysis, Visualization, Writing – review and editing. CR: Formal Analysis, Writing – review and editing. SG: Investigation, Methodology, Supervision, Writing – review and editing.

Funding

The author(s) declared that financial support was not received for this work and/or its publication.

Acknowledgments

The authors acknowledge the use of Grammarly language tools to assist with language improvement during manuscript preparation. The authors take full responsibility for the accuracy and integrity of the work. We also acknowledge Biorender and Canva for creating figures.

Conflict of interest

The author(s) declared that this work was conducted in the absence of any commercial or financial relationships that could be construed as a potential conflict of interest.

Generative AI statement

The author(s) declared that generative AI was not used in the creation of this manuscript.

Any alternative text (alt text) provided alongside figures in this article has been generated by Frontiers with the support of artificial intelligence and reasonable efforts have been made to ensure accuracy, including review by the authors wherever possible. If you identify any issues, please contact us.

Publisher's note

All claims expressed in this article are solely those of the authors and do not necessarily represent those of their affiliated organizations, or those of the publisher, the editors and the reviewers. Any product that may be evaluated in this article, or claim that may be made by its manufacturer, is not guaranteed or endorsed by the publisher.

References

Akinnawo, C. A., and Dube, A. (2025). Clinically relevant metallic nanoparticles in tuberculosis diagnosis and therapy. *Adv. Therapeutics* 8 (4), 2400189. doi: 10.1002/adtp.202400189

Ali, S. S. L., Selvaraj, S., Batoo, K. M., Chauhan, A., Rana, G., Kalaichelvan, S., et al. (2024). Green synthesis of cubic spinel ferrites and their potential biomedical applications. *Ceram. Int.* 50 (24), 52159–52189. doi: 10.1016/j.ceramint.2024.10.084

Ali, M., Irfan, H. M., Alamgeer, Ullah, A., Abdellattif, M. H., Elodemi, M., et al. (2025). Therapeutic role of *Crateva religiosa* in diabetic nephropathy: insights into key signaling pathways. *Plos One* 20 (5), e0324028. doi: 10.1371/journal.pone.0324028

Amigoni-Gerbier, S., Desert, S., Gulik-Kryswicki, T., and Larpent, C. (2002). Ultrafine selective metal-complexing nanoparticles: Synthssis by Micrommulsion Copolcmerization, Bindibg Capaccty, and Liganl Accesaibility. *Macromol.* 35 (5), 1644–1650. doi: 10.1021/ma0113632

Anjum, S., Hashim, M., Malik, S. A., Khan, M., Lorenzo, J. M., Abbasi, B. H., et al. (2021). Recent advances in zinc oxide nanoparticles (ZnO NPs) for cancer diagnosis, target drug delivery, and treatment. *Cancers* 13 (18), 4570. doi: 10.3390/cancers13184570

Anjum, F., Saddiqa, A., Nazir, M. M., Naseer, R., Riaz, M., and Ashraf, A. (2025). Avocado peel-derived polyphenols and date palm mucilage as natural macromolecules in the green synthesis of antimicrobial silver nanoparticles for wound dressing applications. *Int. J. Biol. Macromol.* 329, 147771. doi: 10.1016/j.ijbiomac.2025.147771

Barhoum, A., García-Betancourt, M. L., Jeevanandam, J., Hussien, E. A., Mekkawy, S. A., Mostafa, M., et al. (2022). Review on natural, incidental, bioinspired, and engineered nanomaterials: history, definitions, classifications, synthesis, properties, market, toxicities, risks, and regulations. *Nanomater.* 12 (2), 177. doi: 10.3390/nano12020177

Behzad, F., Sefidgar, E., Samadi, A., Lin, W., Pouladi, I., and Pi, J. (2022). An overview of zinc oxide nanoparticles produced by plant extracts for anti-tuberculosis treatments. *Curr. Med. Chem.* 29 (1), 86–98. doi: 10.2174/0929867328666210614122109

Chaudhary, V., Sonu, S., Taha, B. A., Raizada, P., Rustagi, S., Chahal, S., et al. (2025). Borophene-based nanomaterials: promising candidates for next-generation gas/vapor chemiresistors. *J. Mater. Sci. and Technol.* 218, 236–262. doi: 10.1016/j.jmst.2024.08.038

Chauhan, A., Subbarayan, R., Ravi, K., Verma, R., Rao, S. K., Girija, D. M., et al. (2025). Phytomediated chitosan-modified TiO2 NPs for enhanced photocatalytic and potential application for breast cancer therapy. *Luminescence* 40 (4), e70162. doi: 10.1002/bio.70162

Chavali, M. S., and Nikolova, M. P. (2019). Metal oxide nanoparticles and their applications in nanotechnology. *SN Applied Sciences* 1 (6), 607. doi: 10.1007/s42452-019-0592-3

Chen, E., Chen, C., Chen, F., Yu, P., and Lin, L. (2019). Positive association between MIC gene polymorphism and tuberculosis in Chinese population. *Immunol. Lett.* 213, 62–69. doi: 10.1016/j.imlet.2019.07.008

Cherifi, K., Rekhila, G., Omeiri, S., Bessekhouad, Y., and Trari, M. (2019). *Physical and photoelectrochemical properties of the spinel $ZnCr_2O_4$ prepared by sol gel: application to Orange II degradation under solar light*. *J. Photochem. Photobiol. A Chem.* 368, 290–295. doi: 10.1016/j.jphotochem.2018.10.003

Choudhary, P., Yadav, A., and Varshney, D. (2017). "Structural and optical studies of nanocrystalline $ZnCr_2O_4$ and $CoCr_2O_4$ spinel," in *AIP Conference Proceedings* (Melville, NY: AIP Publishing LLC).

Cuong, H. N., Pansambal, S., Ghotekar, S., Oza, R., Thanh Hai, N. T., Viet, N. M., et al. (2022). New frontiers in the plant extract mediated biosynthesis of copper oxide (CuO) nanoparticles and their potential applications: a review. *A Review. Environ. Res.* 203, 111858. doi: 10.1016/j.envres.2021.111858

Demir Becerekli, H., and Akbaş, F. (2026). Green synthesis, characterization, evaluation of anticancer and antioxidant potentials of gold and copper oxide nanoparticles using jujube fruit extract. *Sci. Rep* 16, 16157. doi: 10.1038/s41598-026-42558-0

Ditlopo, N., Sintwa, N., Khamlich, S., Manikandan, E., Gnanasekaran, K., Henini, M., et al. (2022). From Khoi-San indigenous knowledge to bioengineered CeO_2 nanocrystals to exceptional UV-blocking green nanocosmetics. *Sci. Rep.* 12 (1), 3468. doi: 10.1038/s41598-022-06828-x

Dumitru, R., Manea, F., Păcurariu, C., Lupa, L., Pop, A., Cioablă, A., et al. (2018). *Synthesis, characterization of nanosized $ZnCr_2O_4$ and its photocatalytic performance in the degradation of humic acid from drinking water*. *Catalysts* 8 (5), 210. doi: 10.3390/catal8050210

El Shafey, A. M. (2020). Green synthesis of metal and metal oxide nanoparticles from plant leaf extracts and their applications: a review. *Green Process. Synthesis* 9 (1), 304–339. doi: 10.1515/gps-2020-0031

Elmore, S. (2007). Apoptosis: a review of programmed cell death. *Toxicol. Pathology* 35 (4), 495–516. doi: 10.1080/01926230701320337

Fu, Y., Ni, Y., Cui, W., Fang, X., Chen, Z., Liu, Z., et al. (2023). *Insights into the size effect of $ZnCr_2O_4$ spinel oxide in composite catalysts for conversion of syngas to aromatics*. *Green Energy and Environ.* 8 (2), 530–537. doi: 10.1016/j.gee.2021.07.003

Gene, S. A., Saion, E., Shaari, A. H., Kamarudin, M. A., Al-Hada, N. M., and Kharazmi, A. (2014). Structural, optical, and magnetic characterization of spinel zinc chromite nanocrystallines synthesised by thermal treatment method. *Method. J. Nanomater.* 2014 (1), 416765. doi: 10.1155/2014/416765

Ghotekar, S., Pansambal, S., Nguyen, V. H., Bangale, S., Lin, K. Y. A., Murthy, H. C. A., et al. (2023). *Spinel $ZnCr_2O_4$ nanorods synthesized by facile sol-gel auto combustion method with biomedical properties*. *J. Sol-Gel Sci. Technol.* 105 (1), 176–185. doi: 10.1007/s10971-022-05964-0

Ghotekar, S., Ravikumar, C. R., Chauhan, A., Hikku, G. S., Lin, K. Y. A., Rahdar, A., et al. (2024a). Eco-friendly fabrication of CdO nanoparticles using Polyalthia longifolia leaves extract for antibacterial and electrochemical sensing studies. *J. Sol-Gel Sci. Technol.* 110 (1), 221–232. doi: 10.1007/s10971-024-06352-6

Ghotekar, S., Sanap, D., Patel, K., Abhale, Y., Chauhan, A., Li, L., et al. (2024b). A bio-waste-mediated novel fabrication of ZnCr2O4 nanoparticles: a heterogeneous catalyst in Biginelli reaction. *Res. Chem. Intermed.* 50 (5), 2199–2219. doi: 10.1007/s11164-024-05265-x

Hattiholi, A., Tendulkar, S., Kumbar, V., Rao, M., Kugaji, M., Muddapur, U., et al. (2022). Evaluation of anticancer activities of cranberries juice concentrate in Osteosarcoma cell lines (MG-63). *Indian J. Pharm. Educ. Res.* 56 (4), 1141–1149. doi: 10.5530/ijper.56.4.195

He, Z., Du, J., Wang, Q., Chen, G., Li, X., Zhang, Z., et al. (2024). Dye-augmented bandgap engineering of a degradable cascade nanoreactor for tumor immune microenvironment-enhanced dynamic phototherapy of breast cancer. *Acta Biomaterialia* 176, 390–404. doi: 10.1016/j.actbio.2024.01.007

Heidary, M., Zaker Bostanabad, S., Amini, S. M., Jafari, A., Ghalami Nobar, M., Ghodousi, A., et al. (2019). The anti-mycobacterial activity of Ag, ZnO, and Ag-ZnO nanoparticles against MDR-and XDR-Mycobacterium tuberculosis. *Infect. Drug Resist.* 12, 3425–3435. doi: 10.2147/IDR.S221408

Holzwarth, U., and Gibson, N. (2011). The Scherrer equation *versus* the'Debye-Scherrer equation. *Nat. Nanotechnology* 6 (9), 534. doi: 10.1038/nnano.2011.145

Jadoun, S., Arif, R., Jangid, N. K., and Meena, R. K. (2021). Green synthesis of nanoparticles using plant extracts: a review. *Environ. Chem. Lett.* 19 (1), 355–374. doi: 10.1007/s10311-020-01074-x

Kimta, N., Chauhan, A., Puri, S., Kumari, A., Sharma, R., Kumar, A., et al. (2025). Phytomediated copper oxide nanoparticles derived from the fronds of Adiantum venustum D. Don: evaluation of their biomedical potential. *Appl. Biochem. Biotechnol.* 197 (1), 398–426. doi: 10.1007/s12010-024-05031-0

Kumar, P., Aslam, M., Ali, S., Hamdy, K., Ahmad, K., Danishuddin, (2025). Progress in NiO based materials for electrochemical sensing applications. *Biosensors* 15 (10), 678. doi: 10.3390/bios15100678

Kumari, P. S., Charan, G. V., and Kumar, D. R. (2022). Synthesis, structural, photocatalytic and anti-cancer activity of Zn doped Ni nano chromites by citrate gel auto combustion method. *Inorg. Chem. Commun.* 139, 109393. doi: 10.1016/j.inoche.2022.109393

Lim, E.-K., Kim, T., Paik, S., Haam, S., Huh, Y. M., and Lee, K. (2015). Nanomaterials for theranostics: recent advances and future challenges. *Chem. Rev.* 115 (1), 327–394. doi: 10.1021/cr300213b

Lourenco, M. C., Souza, M. V. N. d., Pinheiro, A. C., Ferreira, M. d. L., Gonçalves, R. S. B., Nogueira, T. C. M., et al. (2007). Evaluation of anti-tubercular activity of nicotinic and isoniazid analogues. *Arkivoc* 15, 181–191. doi: 10.3998/ark.5550190.0008.f18

Lowry, G. V., Avellan, A., and Gilbertson, L. M. (2019). Opportunities and challenges for nanotechnology in the agri-tech revolution. *Nat. Nanotechnology* 14 (6), 517–522. doi: 10.1038/s41565-019-0461-7

Lu, J., Chen, Z., Ma, Z., Pan, F., Curtiss, L. A., and Amine, K. (2016). The role of nanotechnology in the development of battery materials for electric vehicles. *Nat. Nanotechnology* 11 (12), 1031–1038. doi: 10.1038/nnano.2016.207

Mayedwa, N., Mulaudzi-Masuku, T., Matinise, N., and Nkosi, M. (2021). Biosynthesis and characterization of multifunctional mixed oxides of ZnCr2O4/ZnCrO4 nanoparticulate from natural leaf extracts of Hibiscus Rosa Sinensis. *Mater. Today Proc.* 36, 309–312. doi: 10.1016/j.matpr.2020.04.108

Meallet-Renault, R., Hérault, A., Vachon, J. J., Pansu, R. B., Amigoni-Gerbier, S., and Larpent, C. (2006). Fluorescent nanoparticles as selective Cu(II) sensors. *Photochem. and Photobiological Sci.* 5 (3), 300–310. doi: 10.1039/b513215k

Mousavi, Z., Soofivand, F., Esmaeili-Zare, M., Salavati-Niasari, M., and Bagheri, S. (2016). ZnCr2O4 nanoparticles: facile synthesis, characterization and photocatalytic properties. *Scientific Rep.* 6 (1), 20071. doi: 10.1038/srep20071

Munir, H., Bilal, M., Mulla, S. I., Abbas Khan, H., and Iqbal, H. M. (2021). "Plant-mediated green synthesis of nanoparticles," in *Advances in Green Synthesis: Avenues and Sustainability* (Cham: Springer), 75–89.

Ndaba, B., Roopnarain, A., and Maaza, M. (2022). Biosynthesized metallic nanoparticles as fertilizers an emerging precision agriculture strategy. *J. Integr. Agric.* 21 (5), 1225–1242. doi: 10.1016/S2095-3119(21)63751-6

Patel, K., Abhale, Y., Oza, R., Lin, K. Y. A., Larios, A. P., and Ghotekar, S. (2023). "Green silver nanoparticles for nanoremediation," in *Green Nanoremediation: Sustainable Management of Environmental Pollution* (Cham: Springer), 253–274. doi: 10.1007/978-3-031-30558-0_11

Patel, K., Patil, M., Abhale, Y., Lin, K. Y. A., Tan, K. B., Chauhan, A., et al. (2025a). Recent progress on synthesis of $CuCr_2O_4$ nanomaterials and its composites for catalytic, energy, and biomedical applications: a state-of-the-art-review. *Nanoscale* 17 (44), 25426–25476. doi: 10.1039/d5nr03084f

Patel, K., Patil, M., Abhale, Y., Chauhan, A., Rana, G., Adole, V., et al. (2025b). $NiCr_2O_4$ nanomaterials: advances in synthesis, modification, and multifunctional applications. *Inorg. Chem. Commun.* 182, 115451. doi: 10.1016/j.inoche.2025.115451

Patel, K., Patil, M., Abhale, Y., Chauhan, A., Jabir, M. S., Tan, K. B., et al. (2026). Recent advances in synthesis of $ZnCr2O_4$ nanomaterials and its composites for catalytic, energy, sensing, and biomedical applications: a review. *J. Mater. Chem. C* 14 (4), 1308–1359. doi: 10.1039/d5tc03416g

Patil, M., Patel, K., Abhale, Y., Larios, A. P., Kumar, D., Chauhan, A., et al. (2025). New insights in the fabrication of cobalt chromite (CoCr2O4) nanoparticles and their multifunctional applications-a review. *J. Clust. Sci.* 36 (2), 71. doi: 10.1007/s10876-025-02790-6

Peng, H., Luo, M., and Zheng, X. (2024). *Boosting solar-light photocatalytic activity of Ni_2P-decorated $ZnCr_2O_4$ nanofibers for H_2 evolution and tetracycline elimination*. *Ceram. Int.* 50 (15), 26474–26481. doi: 10.1016/j.ceramint.2024.04.375

Priyanka, M., Manjunatha, H. C., Vidya, Y. S., Munirathnam, R., Thirunavukkarasu, V., and Pavithra, B. (2024). Efficient anticancer properties of cerium doped zinc chromite nanoparticles over cisplatin for breast cancer cells. *Appl. Phys. A* 130 (7), 485. doi: 10.1007/s00339-024-07642-0

Pushparaj, K., Liu, W. C., Meyyazhagan, A., Orlacchio, A., Pappusamy, M., Vadivalagan, C., et al. (2022). Nano-from nature to nurture: a comprehensive review on facets, trends, perspectives and sustainability of nanotechnology in the food sector. *Energy* 240, 122732. doi: 10.1016/j.energy.2021.122732

Qiu, S. R., Wood, B. C., Ehrmann, P. R., Demos, S. G., Miller, P. E., Schaffers, K. I., et al. (2015). Origins of optical absorption characteristics of Cu^{2+} complexes in aqueous solutions. *Phys. Chem. Chem. Phys.* 17 (29), 18913–18923. doi: 10.1039/c5cp01688f

Qiu, W., Fan, J., Tao, W., Liang, J., Xiao, C., Chen, Y., et al. (2025). Cinobufagin loaded Prussian blue-like nanoparticles for chemo/gas therapy of multidrug resistant cancer. *J. Nanobiotechnology* 23 (1), 706. doi: 10.1186/s12951-025-03728-w

Rajendaran, K., Muthuramalingam, R., and Ayyadurai, S. (2019). Green synthesis of Ag-Mo/CuO nanoparticles using Azadirachta indica leaf extracts to study its solar photocatalytic and antimicrobial activities. *Mater. Sci. Semicond. Process.* 91, 230–238. doi: 10.1016/j.mssp.2018.11.021

Rana, A., Yadav, K., and Jagadevan, S. (2020). A comprehensive review on green synthesis of nature-inspired metal nanoparticles: mechanism, application and toxicity. *J. Clean. Prod.* 272, 122880. doi: 10.1016/j.jclepro.2020.122880

Rana, G., Dhiman, P., Kumar, A., Selvaraj, S., Chauhan, A., and Sharma, G. (2025). Phytomediated synthesis of Fe3O4 nanoparticles using Cannabis sativa root extract: photocatalytic activity and antibacterial efficacy. *Biomass Convers. Biorefinery* 15 (7), 10275–10292. doi: 10.1007/s13399-024-05785-x

Roy, A., Bulut, O., Some, S., Mandal, A. K., and Yilmaz, M. D. (2019). Green synthesis of silver nanoparticles: biomolecule-nanoparticle organizations targeting antimicrobial activity. *RSC Advances* 9 (5), 2673–2702. doi: 10.1039/c8ra08982e

Salehi, M., Eshaghi, A., and Tajizadegan, H. (2019). *Synthesis and characterization of $TiO_2/ZnCr_2O_4$ core-shell structure and its photocatalytic and antibacterial activity*. *J. Alloys Compd.* 778, 148–155. doi: 10.1016/j.jallcom.2018.11.025

Sankudevan, P., Sakthivel, R. V., Poonkodi, K., Ramalingam, G., Raghupathi, C., Alam, M. M., et al. (2023). *Effects of different precursors on particle size and optical–magnetic properties of $ZnCr_2O_4$ nanoparticles prepared by microwave-assisted method*. *J. Nanomater.* 2023 (1), 2856806–2856809. doi: 10.1155/2023/2856806

Shreyash, N., Bajpai, S., Khan, M. A., Vijay, Y., Tiwary, S. K., and Sonker, M. (2021). Green synthesis of nanoparticles and their biomedical applications: a review. *ACS Appl. Nano Mater.* 4 (11), 11428–11457. doi: 10.1021/acsanm.1c02946

Simões, M. F., Ottoni, C. A., and Antunes, A. (2020). Mycogenic metal nanoparticles for the treatment of mycobacterioses. *Antibiotics* 9 (9), 569. doi: 10.3390/antibiotics9090569

Soni, V., Malhotra, M., Singh, A., Khan, A. A. P., Kaya, S., Katin, K., et al. (2025). Unveiling cutting-edge developments in defective BiOI nanomaterials: precise manipulation and improved functionalities towards bolstered photocatalysis. *Adv. Colloid Interface Science* 340, 103467. doi: 10.1016/j.cis.2025.103467

Tharakeswar, Y., Kalyan, Y., Gangadhar, B., Kumar, K. S. , and Naidu, G. R. (2012). Optical chemical sensor screening cadmium (II) natural waters. *J. Sens. Technol.* 2 (2), 68. doi: 10.4236/jst.2012.22010

Thennarasu, G., and Sivasamy, A. (2015). *Synthesis and characterization of nanolayered ZnO/ZnCr$_2$O$_4$ metal oxide composites and its photocatalytic activity under visible light irradiation*. *J. Chem. Technol. and Biotechnol.* 90 (3), 514–524. doi: 10.1002/jctb.4343

Tural, B., Eslik, G., Ertas, E., Erdogan, O., and Tural, S. (2026). Eco-engineered gold nanoparticles via laurus nobilis at native pH: toward multifunctional nanoformulations for *in vitro* cancer therapy. *Appl. Biochem. Biotechnol.* 198 (4), 2307–2324. doi: 10.1007/s12010-025-05561-1

Vignesh, A., Amal, T. C., Kalaiyarasan, J., Selvakumar, S., and Vasanth, K. (2025). An effective bio-inspired synthesis of palladium nanoparticles using Crateva religiosa G.Forst. leaf extract: a multi-functional approach for environmental and biomedical applications. *Biomass Convers. Biorefinery* 15 (2), 2649–2672. doi: 10.1007/s13399-023-05031-w

Wagay, N., Khan, N., and Rothe, S. (2017). Profiling of secondary metabolites and antimicrobial activity of *Crateva religiosa* G. Forst. bark-A rare medicinal plant of Maharashtra India. *Int. J. Biosci.* 10 (5), 343–354. doi: 10.12692/ijb/10.5.343-8

Wang, Y., Xu, Y., Song, J., Liu, X., Liu, S., Yang, N., et al. (2024). Tumor cell-targeting and tumor microenvironment–responsive nanoplatforms for the multimodal imaging-guided photodynamic/photothermal/chemodynamic treatment of cervical cancer. *Int. Journal Nanomedicine* 19, 5837–5858. doi: 10.2147/IJN.S466042

Wani, T. A., Wani, T. A., G, S., and N, S. (2024). A facile synthesis and characterization of spinel Zinc-Chromite (ZnCr2O4) nanoparticles: their photocatalytic, antibacterial, and anticancer activities. *J. Sol-Gel Sci. Technol.* 110 (1), 74–89. doi: 10.1007/s10971-024-06346-4

Yazdanbakhsh, M., Khosravi, I., Goharshadi, E. K., and Youssefi, A. (2010). *Fabrication of nanospinel ZnCr$_2$O$_4$ using sol–gel method and its application on removal of azo dye from aqueous solution*. *J. Hazardous Materials* 184 (1-3), 684–689. doi: 10.1016/j.jhazmat.2010.08.092

Yu, X., Marks, T. J., and Facchetti, A. (2016). Metal oxides for optoelectronic applications. *Nat. Materials* 15 (4), 383–396. doi: 10.1038/nmat4599

Zeng, X., Hou, Y., Luo, L., Ren, L., Wang, Y., Jin, X., et al. (2025). Multifaceted roles of heparin and its derivatives in inflammation and cancer: mechanisms, clinical applications, and future directions. *Int. J. Biol. Macromol.* 330, 148054. doi: 10.1016/j.ijbiomac.2025.148054

Zhao, L., Zhou, C., Zhou, Y., Wang, T., Liu, F., Yan, X., et al. (2023). Simple preparation of yolk-shell ZnCr2O4 microspheres and their application to xylene gas sensor. *Sensors Actuators B Chem.* 390, 133929. doi: 10.1016/j.snb.2023.133929